Appl. Phys. B 81, 363–367 (2005)
DOI: 10.1007/s00340-005-1865-7

Applied Physics B
Lasers and Optics

M.A. FOSTER[1]
J.M. DUDLEY[2,✉]
B. KIBLER[2]
Q. CAO[3]
D. LEE[3]
R. TREBINO[3]
A.L. GAETA[1]

Nonlinear pulse propagation and supercontinuum generation in photonic nanowires: experiment and simulation

[1]School of Applied and Engineering Physics, Cornell University, Ithaca NY, 14853, USA
[2]Institut FEMTO-ST, Départément d'Optique P.M. Duffieux, CNRS UMR 6174, Université de Franche-Comté, 25030 Besançon, France
[3]School of Physics, Georgia Institute of Technology, Atlanta GA, 30332-0430, USA

Received: 18 February 2005
Published online: 15 July 2005 •

ABSTRACT We investigate theoretically and experimentally the process of supercontinuum generated in sub-wavelength waveguides. We observe experimentally that supercontinuum generated in these photonic nanowires is increasingly blue-shifted from the pump wavelength for decreasing minimum core diameters. We also find the spectral features are sensitive to the specific nanowire profile. Numerical simulations using the nonlinear envelope equation show that accurate modeling requires consideration of the nonlinearity and full dispersion along the entire nanowire profile as well as a wavelength dependent loss. Specifically, the blue-shifting is found to result from an increasing loss for wavelengths larger than the core diameter.

PACS 42.65.−k; 42.81.Dp

1 Introduction

Since the first demonstration of supercontinuum generation (SCG) in micro-structured and tapered fibers [1, 2], much research was conducted to understand and control the process. This research lead to breakthrough applications in such fields as optical frequency metrology and optical coherence tomography [3–6]. Two properties of these fibers make them ideally suited to efficient broadband nonlinear frequency generation. The large index contrast of glass (1.45) to air (1.0) and small core diameters of approximately 2 μm provide high modal confinement and a significant waveguide contribution to the dispersion. With the appropriate choice of waveguide parameters, high effective nonlinearities are achieved with low group-velocity dispersion (GVD) at the pump wavelength [7–9]. While researchers have investigated extensively the control of the nonlinear interaction by altering the GVD of fibers with core diameters larger than the pump wavelength, more recently the regime of sub-wavelength diameter waveguides has attracted interest [10, 11]. Waveguides of sub-wavelength diameters, known as photonic nanowires, can provide maximal effective nonlinearities as well as exotic dispersion profiles [12–14]. Fabrication of low-loss nanowires was demonstrated using various techniques [11–19]. Specifically, durable sub-wavelength waveguides were fabricated by tapering standard micro-structured fibers such that the core diameter becomes sub-wavelength in scale. The outer diameter of these fibers is tens of microns making them robust to manipulation as well as to changes in their environment. Using these fibers, ultra-efficient octave spanning SCG was demonstrated using both nanosecond and femtosecond pump pulses [16, 17]. This continuum is characterized by a blue-shifted spectrum generated well into the visible with little spectral power in the infrared. Understanding of the dynamics leading to these characteristic spectra will allow for greater control and applicability of nanowire generated supercontinua.

In this paper, we investigate ultrafast pulse propagation dynamics in photonic nanowires. We measure the supercontinuum generated in three waveguides with different core diameters. Experimentally, we find a the continuum shifts to the blue and the propagation loss in the infrared increases as the core diameters are decreased. We perform simulations using the nonlinear envelope equation to elucidate the propagation dynamics within the fiber. We find that consideration of the shape of the taper profile and inclusion of the full dispersion and wavelength dependent loss are necessary to achieve agreement with the experimental results.

2 Waveguiding properties of nanowires

2.1 *Effective nonlinearity*

The properties of the high air-filling-fraction micro-structured fibers used for SCG are adequately modeled as a glass core surrounded by an air cladding [20]. With this model, we analyzed the confinement of the fundamental mode as the size of the core is reduced [14]. As seen in Fig. 1, for cores larger than the wavelength of propagating light, the mode field diameter (MFD) follows the core diameter. However, as the core becomes smaller than the wavelength of light, the MFD reaches a minimum and then diverges rapidly. This behavior leads to a specific waveguide diameter which

✉ Fax: +33-3-81-66-64-23, E-mail: john.dudley@univ-fcomte.fr

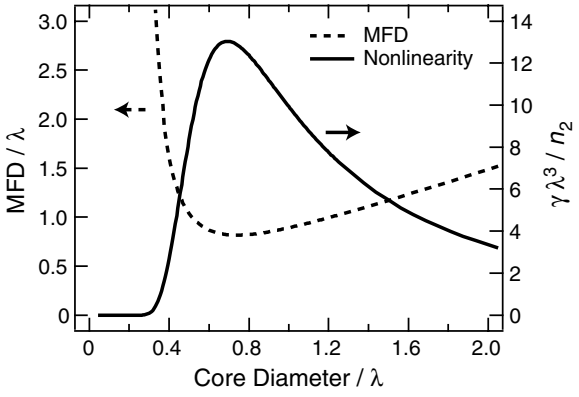

FIGURE 1 The mode field diameter (MFD) and the normalized effective nonlinearity $\gamma\lambda^3/n_2$ for a circular glass (index of 1.45) waveguide in air (index of 1.0)

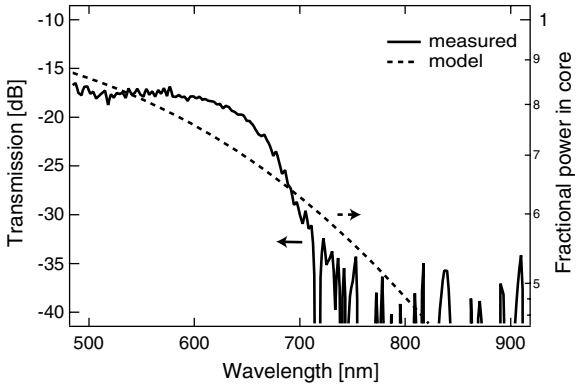

FIGURE 3 Measured transmission and calculated fractional power in the core for a 400-nm waist diameter tapered microstructured fiber. μm

maximizes the effective nonlinearity (see Fig. 1) and we find that the maximally nonlinear waveguide is sub-wavelength in size. For example, for 800-nm light produced by a Ti:sapphire laser, a fiber core diameter of 550 nm optimizes the nonlinearity.

2.2 *Group-velocity dispersion*

The sensitive dependence of the MFD to the core diameter yields a substantial waveguide contribution to the group-velocity dispersion (GVD). Using the glass-rod-in-air model, we calculated the GVD of several sub-wavelength waveguides, and the results are shown in Fig. 2. For the 2.3-μm-core waveguides commonly used for SCG, the first zero-GVD point is shifted into the visible while the second zero-GVD point lies in the infrared. For nanowires, the larger waveguide contribution to the GVD pushes both zeros into the visible [13, 14]. With the appropriate choice of the core size, the second zero-GVD point can be positioned near the pump wavelength to yield anomalous, normal, or zero GVD.

2.3 *Wavelength dependent loss*

For sub-wavelength waveguides, a significant fraction of the modal power resides in the evanescent field. This portion of the mode is interacting directly with the air-glass interfaces. Any imperfections in this structure, such as surface roughness, will lead to scattering and loss [21, 22]. For longer wavelengths, a larger fraction of the power lies in the evanescent field, therefore one would expect a larger loss. For example, Fig. 3 shows the calculated fractional power in the core as compared to the measured transmission of a tapered microstructured fiber with a 400-nm minimum core diameter. In this case, the relative loss becomes significant for wavelengths with more than a 25 percent of the power in the evanescent field.

3 Experiment

The method by which we fabricate sub-wavelength waveguides was described previously [15–17]. The technique consists of tapering a 2.3-μm core microstructured fiber using a standard flame-brush technique [23] such that the microstructured cladding remains intact. By this method, the core is reduced to a sub-wavelength size over a few centimeter region. The taper profiles used in this investigation are shown in Fig. 4. Fibers A and B have similar profiles but different minimum waist diameters of 400 nm and 500 nm, respectively. Fiber C is shorter in length and has a larger minimum waist diameter of 775 nm. Furthermore, Fibers A and B have a centrally located taper with a total fiber length of

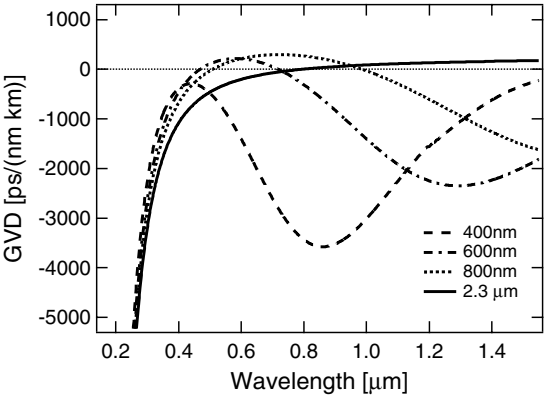

FIGURE 2 Group-velocity dispersion (GVD) of a glass rod in air for core diameters of 400 nm, 600 nm, 800 nm, and 2.3 μm

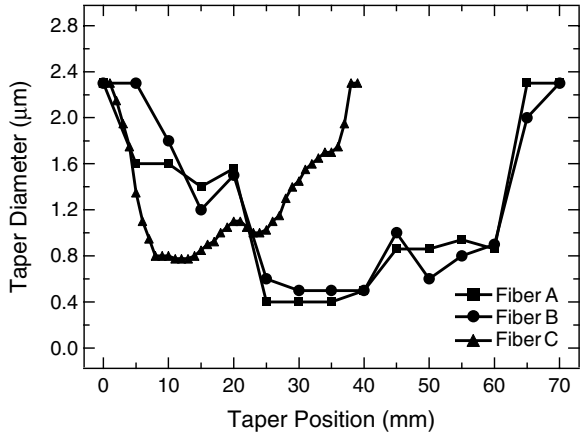

FIGURE 4 Core diameter profiles of the tapered microstructured fibers used in this investigation

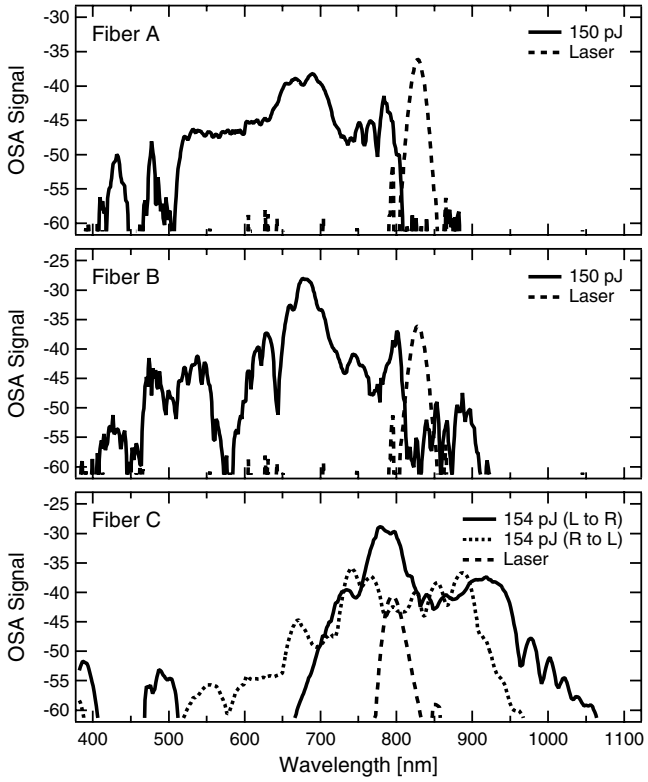

FIGURE 5 Generated spectra and input spectra for the three tapered microstructured fibers described in Fig. 4

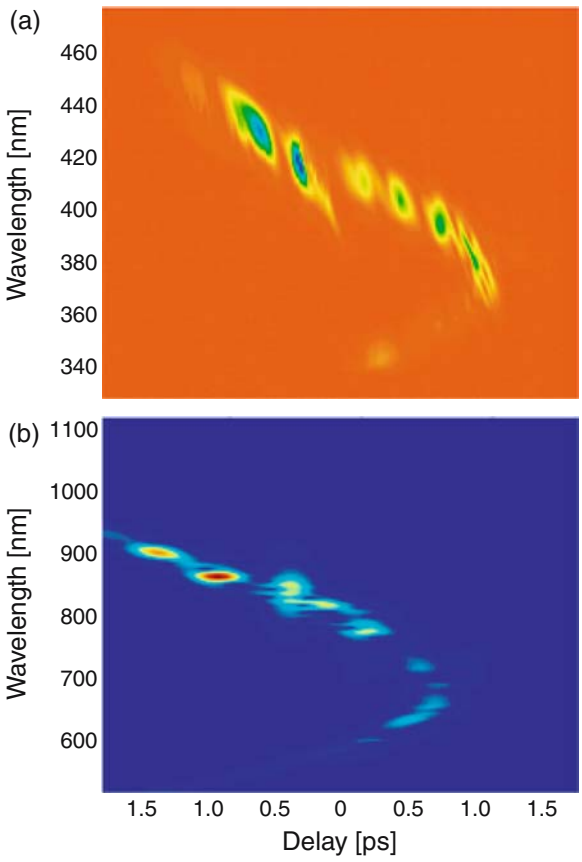

FIGURE 6 Spectrogram representation of supercontinuum generated in fiber C, **a** measured using cross-correlation frequency resolved optical gating (XFROG) and, **b** simulated using the nonlinear envelope equation

20 cm. Fiber C has 56 mm of untapered fiber to the left of the taper and 83 mm to the right.

Supercontinuum was generated in these fibers using femtosecond pulses from a mode-locked Ti:Sapphire laser. For fibers A and B, the input pulse was 25 fs in duration with an energy of 150 pJ inside the fiber. For fiber C, the input pulse was 35 fs in duration with a pulse energy of 154 pJ inside the fiber. The generated spectra are shown in Fig. 5. The continuum generated in fibers A and B is substantially blue-shifted from the pump wavelength, whereas the continuum from Fiber C is not. This will be shown to be a result of the significant wavelength dependent loss for fibers with small minimum core diameters. Additionally, continuum was generated by traveling both left to right and right to left through fiber C. Unique spectra are generated for each direction of propagation which illustrates the dependence of the continuum on the taper profile. For fibers A and B both the propagation direction was left to right.

The supercontinuum generated in Fiber C was further analyzed using cross-correlation frequency resolved optical gating (XFROG) [18]. This measurement yields a spectrogram representation of the generated supercontinuum pulse, see Fig. 6. This measurement was made on supercontinuum generated using 163 fs pulses with a 800 nm central wavelength and 190 pJ pulse energy from a Ti:Sapphire oscillator. The spectrogram representation gives insight into the temporal properties of the generated spectral components. As will be explained in Sect. 4.2, spectral components in tapered microstructured fibers are generated in two stages. Spectral broadening initially occurs in the microstructured fiber before the taper. Solitons are formed which are then dispersed temporally. When this supercontinuum pulse enters the tapered region, the solitons are exposed to a new dispersive regime which causes some to break up and spectrally broaden in the same way as the initial input pulse in the untapered fiber. This multiple staged SCG process leads to the branching of the spectrogram seen near 0 delay in Fig. 6.

4 Simulation

4.1 *Pulse propagation model*

A number of groups have demonstrated that the ultrafast pulse propagation dynamics of SCG in microstructured fibers are successfully analyzed using the nonlinear envelope equation [8, 9, 24]. The adaptation of this approach to model SCG in the nanowires studied here is relatively straightforward, requiring only that the longitudinal variation of the fiber diameter as a function of propagation distance is accurately taken into account through its effect on the fiber dispersion, nonlinearity, and loss.

The fiber dispersion requires particular care because the GVD varies greatly over the supercontinuum bandwidth (as seen in Fig. 2), the usual Taylor series approach is not useful, and accurate modeling requires inclusion of the full dispersion profile. In addition, because propagation in nanowires is influenced by the wavelength dependent loss, this effect must

be included to obtain accurate results in the sub-wavelength regime. In our simulations, we use a physically justified yet empirical model for the loss in which it is proportional to the amount of power in the evanescent field. We find that inclusion of this property was necessary for accurate modeling of the supercontinuum generated in the fibers with 400-nm and 500-nm minimum core diameters. However, we found that this loss mechanism was not necessary to accurately model SCG in fibers with minimum diameters exceeding 775-nm. As seen in Fig. 1, nanowires also have a wavelength dependence to the effective nonlinearity, nevertheless inclusion of this property was shown to yield only a minor correction to the generated spectrum [25], and we verified that its contribution in the parameter regime studied here was negligible.

4.2 *Comparison with experiment*

The simulations were used to model the two particular experimental cases for Fiber A and Fiber C as described above. The parameters used in the simulations corresponded to those in the experiments with no free parameters. Figure 7 shows the results obtained that illustrate very clearly the general differences observed between the two fibers. Although the pump wavelengths are identical in the two cases, the output spectra exhibit very different wavelength-dependence. In particular, the results for Fiber A clearly reproduce the strong spectral blue-shift, whereas the results for Fiber C exhibit features more characteristic of SCG in untapered microstructure fibers where the spectrum is red-shifted due to the Raman self-frequency shift. Our simulations allow us to clarify the particular mechanism responsible for these differences as the wavelength-dependence of the taper loss. For the sub-wavelength case of Fiber A, it strongly attenuates the red-shifted components relative to the blue whereas for Fiber C, its effect has been confirmed to be negligible.

The new features of SCG in a sub-wavelength taper can be illustrated clearly using the spectrogram representation of the

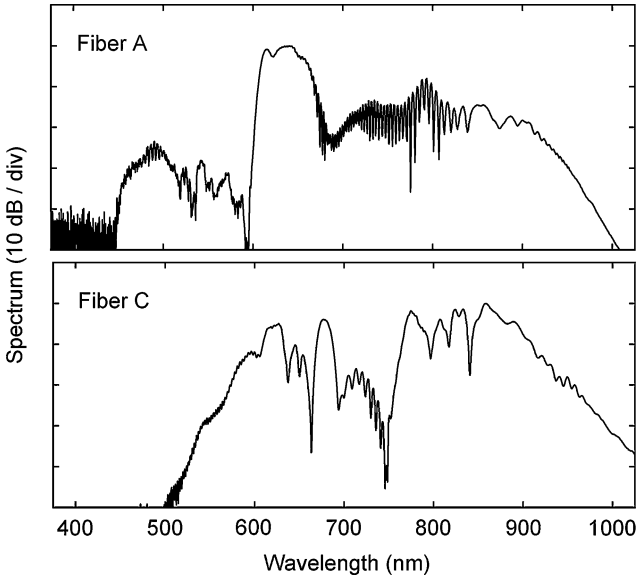

FIGURE 7 Simulated spectra for **a** Fiber A and **b** Fiber C as described in the text

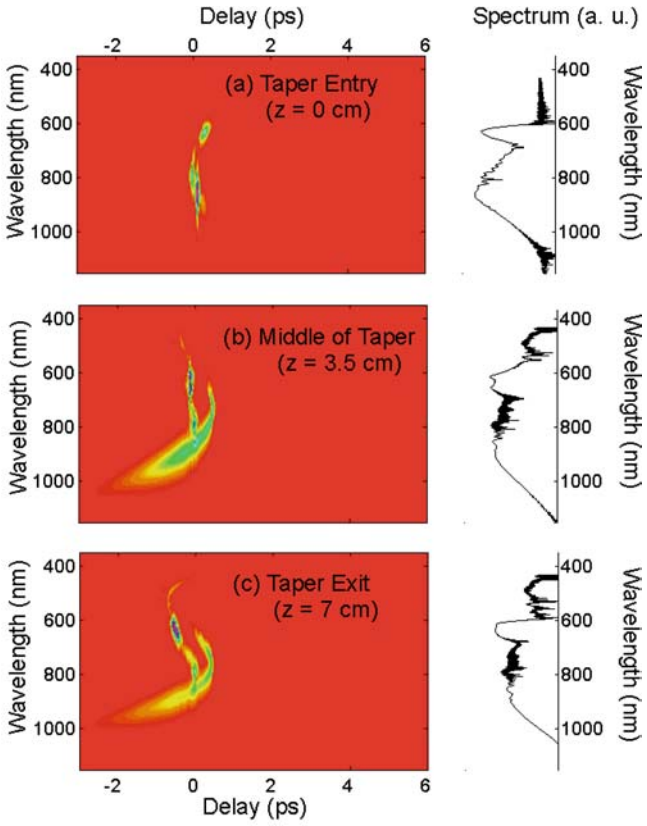

FIGURE 8 Spectrogram (*and projected spectral*) evolution in the sub-wavelength taper region of Fiber A at propagation distances as shown

evolving pulse. Figure 8 shows the calculated spectrogram at three positions in the tapered region. At the taper input, the spectrum is typical of those commonly observed in microstructure fiber SCG experiments at low power where the input pulse has undergone some spectral broadening and non-solitonic blue-shifted dispersive wave generation occurs. As this field encounters the enhanced nonlinearity and modified dispersion in the sub-wavelength diameter region, however, the spectrum changes significantly. The combination of the modified dispersion and loss at longer wavelengths disperses and attenuates the long wavelength edge of the spectrum and, most significantly, new spectral components are generated between 400–600 nm, a wavelength regime difficult to access through Kerr nonlinear processes using untapered microstructure fiber. Physically, the generation of this radiation arises because, in the sub-wavelength region, the radiation generated between 600–800 nm in the initial phase of SCG now propagates in the anomalous GVD regime and can induce further dispersive wave generation to generate blue-shifted radiation in the range 450–500 nm where the GVD is normal for taper diameters < 1 μm. These GVD properties can be seen in Fig. 2 and are also reflected in the spectrogram shape that indicates the group delay of the propagating field.

5 Conclusion

We have shown that the blue-shifting of a nanowire generated supercontinuum is a function of the minimum core diameter of the waveguide. We investigated the ultrafast pulse

propagation dynamics of photonic nanowires using the nonlinear envelope equation, and accurate results were achieved only by taking into account the position dependence of the nonlinearity, the full dispersion profile, and a wavelength-dependent loss. This loss is found to be the primary cause for the observed blue-shifted supercontinuum in the case of a sub-wavelength taper. A detailed understanding of the pulse propagation dynamics of nanowires is necessary to facilitate their implementation into photonic devices. In particular, the understanding gained in this investigation will allow for designing nanowires which generate tailored spectral or temporal features.

REFERENCES

1 J.K. Ranka, R.S. Windeler, A.J. Stentz, Opt. Lett. **25**, 25 (2000)
2 W.J. Wadsworth, A. Ortigosa-Blanch, J.C. Knight, T.A. Birks, T.P.M. Man, P.St.J. Russell, J. Opt. Soc. Am. B **19**, 2148 (2002)
3 D.J. Jones, S.A. Diddams, J.K. Ranka, A. Stentz, R.S. Windeler, J.L. Hall, S.T. Cundiff, Science **288**, 635 (2000)
4 S.A. Diddams, D.J. Jones, J. Ye, S.T. Cundiff, J.L. Hall, J.K. Ranka, R.S. Windeler, R. Holzwarth, T. Udem, T. Hänsch, Phys. Rev. Lett. **84**, 5102 (2000)
5 I. Hartl, X.D. Li, C. Chudoba, R.K. Ghanta, T.H. Ko, J.G. Fujimoto, J.K. Ranka, R.S. Windeler, Opt. Lett. **26**, 608 (2001)
6 F. Quochi, M. Dinu, L.N. Pfeiffer, K.W. West, C. Kerbage, R.S. Windeler, B.J. Eggleton, Phys. Rev. B **67**, 235323 (2003)
7 A.V. Husakou, J. Herrmann, Phys. Rev. Lett. **87**, 203901 (2001)
8 A.L. Gaeta, Opt. Lett. **27**, 924 (2002)
9 J.M. Dudley, S. Coen, Opt. Lett. **27**, 1180 (2002)
10 D. Akimov, M. Schmitt, R. Maksimenka, K. Dukel'skii, Y. Kondrat'ev, A. Khokhlov, V. Shevandin, W. Kiefer, A. Zheltikov, Appl. Phys. B **77**, 299 (2003)
11 L.M. Tong, R.R. Gattass, J.B. Ashcom, S.L. He, J.Y. Lou, M.Y. Shen, I. Maxwell, E. Mazur, Nature **426**, 816 (2003)
12 A.M. Zheltikov, Optics and Spectroscopy **95**, 410 (2003)
13 L.M. Tong, J.Y. Lou, E. Mazur, Opt. Express **12**, 1025 (2004)
14 M.A. Foster, K.D. Moll, A.L. Gaeta, Opt. Express **12**, 2880 (2004)
15 E.C. Mägi, P. Steinvurzel, B.J. Eggleton, Opt. Express **12**, 776 (2004)
16 S. Leon-Saval, T. Birks, W. Wadsworth, P. Russell, M. Mason, Opt. Express **12**, 2864 (2004)
17 M.A. Foster, A.L. Gaeta, Opt. Express **12**, 3137 (2004)
18 J.M. Dudley, X. Gu, L.Xu, M. Kimmel, E. Zeek, P. O'Shea, R. Trebino, S. Coen, R.S. Windeler, Opt. Express **10**, 1215 (2002)
19 Y. Lize, E.C. Mägi, V. Ta'eed, J. Bolger, P. Steinvurzel, B. Eggleton, Opt. Express **12**, 3209 (2004)
20 J. Knight, J. Arriaga, T. Birks, A. Ortigosa-Blanch, W. Wadsworth, P. Russell, IEEE Photon. Technol. Lett. **12**, 807 (2000)
21 V. Finazzi, T.M. Monro, D.J. Richardson, IEEE Photon. Technol. Lett. **15**, 1246 (2003)
22 E.C. Mägi, H.C. Nguyen, B.J. Eggleton, Opt. Express **13**, 453 (2005)
23 T.A. Birks, Y.W. Li, J. Lightwave Technol. **10**, 432 (1992)
24 T. Brabec, F. Krausz, Phys. Rev. Lett. **78**, 3283 (1997).
25 M. Kolesik, E. Wright, J. Moloney, Appl. Phys. B **79**, 293 (2004)